



Ni-Co catalyst-assisted carbon cycling for CH₄-CO₂ reforming

Jiangyong Yuan ^{a,b}, Chunqiang Lu ^{a,b}, Zhenhua Gu ^c, Jun Cai ^{a,b}, Han Zhao ^{a,b}, Danyang Li ^{a,b}, Lei Jiang ^{a,b}, Haiwen Xu ^{a,b}, Zhi qiang Li ^{a,b,*}, Kongzhai Li ^{a,b,*}

^a Engineering Research Center of Metallurgical Energy Conservation and Emission Reduction, Ministry of Education, Kunming University of Science and Technology, Kunming 650093, China

^b National Joint Engineering Research Center of Energy Saving and Environmental Protection Technology in Metallurgy and Chemical Engineering Industry, Kunming University of Science and Technology, Kunming 650093, China

^c School of Energy and Environment Science, Yunnan Normal University, Kunming 650093, Yunnan, China



ARTICLE INFO

Keywords:

Chemical looping
Carbon deposition
Carbon cycling
Ni-Co alloy

ABSTRACT

Carbon cycling, instead of conventional oxygen cycling in chemical looping, overcomes the limitations of oxygen storage capacity of oxygen carriers and enables the reaction to proceed under relatively mild conditions. In this study, we designed a high-performance carbon-storage catalyst (Ni-Co/Al₂O₃) for chemical looping conversion of CH₄ and CO₂ to H₂ and CO. The physico-chemical characterizations suggested that the Co alloyed with Ni could result in larger active metal particles and simultaneously benefit the bending of carbon deposits toward the periphery of the active sites, avoiding the quick deactivation of catalysts due to the encapsulation of the active sites by carbon deposits and generating a higher carbon capacity (23.59 vs. 14.08 mol/kg). In addition, the alloying of Co with Ni could weaken the graphitization of carbon deposits, thus facilitating the carbon elimination and catalyst regeneration in the CO₂ conversion step, strongly improving the cycling stability during long-term testing.

1. Introduction

Fossil fuels have brought about an era of unprecedented prosperity for human society, while the increase in anthropogenic CH₄ and CO₂ emissions has many negative impacts [1–3]. Furthermore, as a finite and non-renewable resource, the unsustainability of fossil fuels will ultimately force people to search for alternative sources of new energy [1, 4].

In this global industrial transformation revolution, C1 small molecules represented by CO₂, CO, and CH₄ are expected to play a variety of important roles, including raw materials, intermediates and platform compounds [2,4–7]. CH₄ and CO₂ are widely exploited as cheap sources of carbon due to their abundant and relatively inexpensive natural reserves [2–4,8]. Chemical looping methane dry reforming as a novel technology enables the conversion of CH₄ to syngas, coupled with CO₂ splitting to produce CO [8–11]. This can transform the two major greenhouse gases to syngas with variable CO/H₂ ratios for various industrial processes such as methanol synthesis, hydroformylation and Fischer-Tropsch reaction. Since it is a strong endothermic reaction, this

is also an energy storage process when renewable energy is used to supply heat [12,13]. It is noteworthy that such an oxygen cycling technology reported to date typically requires high temperature conditions (>800 °C) to achieve oxygen cycling with metal oxides as oxygen carriers [8,11]. This is essentially attributed to the low surface activity for methane activation and the high activation energy required for lattice oxygen transport and cation migration in the oxygen carrier. Furthermore, as the lattice oxygen in the metal oxide is gradually depleted in the syngas production process, carbon deposits will inevitably form, resulting in low syngas yields, poor H/C ratios and inefficient CH₄ utilization [10]. Therefore, the ability to store and migrate oxygen in the metal oxide lattice is central to this technology [11]. However, some studies have found that carbon species on the oxygen carrier during the methane reforming step could be eliminated by charging H₂O or CO₂ during the oxidation step [14–16]. It was reported that the reaction between CO₂ and carbon was favored above 700 °C [17]. Therefore, it is highly desirable to develop a process that employs carbon species to improve CO₂ splitting while more effective CH₄ utilization.

In order to break the limitations of the oxygen release capacity of

* Corresponding author at: Engineering Research Center of Metallurgical Energy Conservation and Emission Reduction, Ministry of Education, Kunming University of Science and Technology, Kunming 650093, China.

E-mail addresses: kongzhai.li@foxmail.com, kongzhai.li@aliyun.com (K. Li).

metal oxides for chemical looping methane dry reforming technology, a carbon cycling process using methane cracking coupled with CO₂ splitting has been proposed to substitute for the metal oxide cycling [17, 18]. Further improvements are made based on the methane conversion chemical cycle process to produce separated H₂ and CO. In a cracking reactor, CH₄ is catalyzed by a metal catalyst to produce H₂ flow and solid carbon deposited on the catalyst. In an oxidation reactor, CO₂ is used as an oxidant to selectively oxidize the deposited carbon to produce CO, then the regenerated metal catalyst is recycled back to the cracking reactor. As a result, the catalyst circulates between the two independent reactors, producing separated H₂ and CO streams. During chemical looping, characteristic oxygen carriers become carbon carriers to present the carbon cycle [17]. This technology can utilize carbon species for CO₂ splitting, unlike the catalytic decomposition of methane for hydrogen production, which will lead to catalyst decay and deactivation due to carbon deposition. Some studies have reported Ni/Al₂O₃ as a catalyst for this system, with poor stabilization and rapid deactivation caused by carbon deposits. Moreover, studies using Ni/La₂O₃ [17] and Ni/CeO₂ [18] as carbon carriers have also been conducted, which achieved nearly 100% conversion of methane. However, the operation temperature was required over 800 °C, which result in high energy consumption and easy sintering of catalysts. Exploring carbon carriers that can react under relatively mild conditions with high reactivity and stability is the key to promoting this technology. Consequently, it is necessary to explore efficient, economical and stable catalysts for CH₄ cracking coupled with CO₂ decomposition to enable the carbon cycling.

Noble metal catalysts have shown good stability and coking resistance, but high costs have prevented their extensive application [7]. With comparable activity to that of noble metal catalysts, nickel-based catalysts are of interest because of its ability for efficient cleavage of C-H bonds, easy availability and low cost among the non-noble metals [19–21]. However, high reaction temperatures could lead to deactivation of the nickel catalysts due to agglomeration, sintering and chemical poisoning, thus hindering their further application. Therefore, it is desirable to enhance the catalyst performance by investigating bimetallic catalysts to alleviate particle sintering and facilitate carbon elimination. The interactions between metals in the bimetallic catalysts provide different physicochemical properties from the parent metal, thus improving the activity, selectivity and stability of the catalyst [22–24]. Many studies have indicated that the coking problems of nickel-based catalysts can be significantly alleviated by the incorporation of cobalt [20,25–27], and the oxygen affinity of the Co-Ni bimetallic catalysts can also be altered due to the addition of cobalt [23]. Since Co has a strong affinity for oxygen, the Co-O interaction could enhance CO₂ adsorption, which is conducive to carbon species elimination from the catalyst surface. [20,28,29]. On the other hand, support materials will play a great role in catalyst modification, and many reports have investigated the effect of various support materials such as Al₂O₃ [30], SiO₂ [20], La₂O₃ [17], MgAl₂O₄ [22], CeO₂ [31] and ZrO₂ [19]. Due to its mechanical and chemical stability at high temperatures, γ-Al₂O₃ has been commonly used as a catalyst carrier [30]. Furthermore, the large specific surface area of the γ-Al₂O₃ carrier could provide a high dispersibility of the active metal and the inhibition of particle agglomeration and sintering, thus promoting the gas-solid reaction.

In this study, methane cracking combined with a CO₂ splitting process based on chemical looping technology was tested at relatively mild temperatures with Co-Ni/Al₂O₃ catalysts. The whole reaction process mainly involved the consumption and replenishment of carbon, which could break the limitations of the oxygen storage and release performance of conventional metal oxides. A series of activity evaluations and physicochemical characterization tests have shown that the introduction of Co to form a Ni-Co alloy can effectively boost the carbon capacity and carbon build-up elimination simultaneously, thereby enabling excellent activity and stability of the catalyst.

2. Experimental

2.1. Catalyst preparation

A series of Co-Ni/γ-Al₂O₃ catalysts were prepared by wet impregnation. The total mass of Co and Ni loading (25%) was maintained, and the proportion of component Co and Ni loading was varied. The Co (NO₃)₂·6H₂O (Aladdin) and Ni(NO₃)₂·6H₂O (Aladdin) with varying proportions were dissolved in deionized water, followed by stirring well and addition of γ-Al₂O₃ (Aladdin) powder. The mixture was dried in a water bath at 70 °C. After that, the prepared samples were further dried in a vacuum oven under room temperature for 12 h and then calcined in a muffle furnace under air atmosphere at 700 °C for 3 h with a rate of 5 °C/min. The Co-Ni/γ-Al₂O₃ catalysts were labeled as xNi_yCo, where x indicated the mass percentage of Ni loading and y referred to that of Co, and the catalysts were named as 21Ni4Co, 17Ni8Co, 13Ni12Co and 9Ni16Co. Specially, the samples with only Co or Ni were named as 25Co or 25Ni, respectively.

2.2. Characterizations

X-ray diffraction (XRD, Rigaku Miniflex 600) patterns were recorded with an excitation source of Cu-Kα radiation, and the λ was 0.15406 nm with a tube current and voltage of 40 kV and 20 mA. The scan range of the sample was set from 10° to 90° with a speed of 5 °/min.

Hydrogen temperature-programmed reduction (H₂-TPR) and CO₂ temperature-programmed desorption (CO₂-TPD) experiments were carried out on a TPR/TPD setup (Quantachrome Instrument). H₂-TPR was performed in a U-shaped quartz tube filled with 0.1 g of sample and pre-treated by charging 30 mL/min of high purity helium at 200 °C for 1 h with a rate of 10 °C/min. A 10 vol% H₂/Ar mixture gas was then introduced at a rate of 10 °C/min with a gas flow of 30 mL/min until 800 °C. CO₂-TPD was performed by pre-treating 0.1 g of sample in a U-shaped quartz tube with high purity helium at a constant temperature of 200 °C for 1 h, followed by cooling to room temperature. After purging with helium, the tube was charged with 5 vol% CO₂ in equilibrium with argon at a rate of 200 mL/min, while the sample was ramped from 40 °C to 800 °C at a rate of 10 °C/min.

CH₄ temperature-programmed reaction (CH₄-TPR) was carried out on a small fixed bed reactor. After purging 0.2 g of sample in quartz tube with argon, 5 vol% CH₄ in equilibrium with Ar was flowed into the tube at a rate of 200 mL/min, and the sample was heated from 40 °C to 800 °C with a ramp of 10 °C/min. The CO₂ temperature-programmed oxidation (CO₂-TPO) experiment was similar to CH₄-TPR, except that 5 vol% CO₂/Ar (200 mL/min) was used in CO₂-TPO. A mass spectrometer (MS) was used in order to detect the exit gas.

X-ray photoelectron spectroscopy (XPS) tests were performed on an apparatus (K-Alpha, Thermo Fisher Scientific) equipped with an X-ray excitation source Al Kα-rays ($\text{hv}=1486.6 \text{ eV}$). The analysis chamber vacuum was better than $5.0 \times 10^{-7} \text{ mbar}$ and the operating voltage was 12 kV. A C1s binding energy of 284.80 eV was used as the energy standard for the binding energy correction.

Raman spectroscopy measurements were conducted on a micro Raman spectrometer (DXRxi type, Thermo Fisher Scientific). The laser wavelength was 532 nm and the detection frequency range was in the range of 1000–2000 cm⁻¹.

Transmission electron microscopy (TEM) and high-resolution TEM measurements were carried out on a TEM device (Tecnai G² TF30 S-Twin), along with for acquiring HAADF images, mapping and elemental line scans. The test samples were crushed into powder and immersed in ethanol for sonication and dispersion. A small drop of the suspension was placed on a multi-copper grid and dried for testing.

2.3. Reaction tests

The performance of the sample was tested in a fixed bed reactor

under atmospheric pressure. Typically, 0.5 g of catalyst (20–40 mesh) in a quartz tube (10 mm in diameter) was placed in a tube furnace. Firstly, the catalyst was heated from room temperature to 300 °C at a rate of 5 °C/min and kept for 30 min in high purity N₂ to remove the possible impurities on the catalysts and then raised to 700 °C. Thereafter, the sample was reduced with 10 vol% H₂/N₂ at 700 °C for 30 min and then purged with high purity N₂ before activity testing. Then 5%vol CH₄/N₂ (200 mL/min) was fed into the reactor to react over the catalyst for 30 min. After the methane cracking reaction, the reactor was purged clean with high purity N₂. Then in the CO₂ splitting stage, 5 vol% CO₂/N₂ (150 mL/min) was fed into the reactor to react with the carbon deposited on the catalyst to produce CO. Quantitative analyses of the main products and reactants were performed by combining a gas chromatograph (GC, Agilent 7890) and a non-dispersive infrared radiation (NDIR) gas analyzer (GASBOARD-3100, Wuhan Cubic Optoelectronics Co., Ltd.).

In the continuous chemical looping cycle stability test, the catalyst (0.5 g) was regenerated by charging 5 vol% CO₂ (200 mL/min) into the reactor after the reduction reaction with a feed of 5 vol% CH₄ (200 mL/min) for 5 min. The outlet gases were monitored by a mass spectrometer. Between each step, the reactor was purged with high purity argon (200 mL/min) for ~10 min to avoid gas mixing.

The average CH₄ conversion (X_{CH₄}), the selectivity of H₂ (S_{H₂}), CO₂ (S_{CO₂}), CO (S_{CO}), and coke (S_{Coke}), H₂ yield (Y_{H₂}) and carbon capacity during the CH₄ conversion step, and the average CO₂ conversion (X_{CO₂}) and CO yield (Y_{CO}) during the CO₂ splitting step are calculated by the following equations.

Average CH₄ conversion:

$$X_{CH_4} (\%) = \frac{\int_0^t C_{CH_4,in} dt \times F - \int_0^t C_{CH_4,out} dt \times F}{\int_0^t C_{CH_4,in} dt \times F} \quad (1)$$

Average H₂ selectivity:

$$S_{H_2} (\%) = \frac{\int_0^t C_{H_2,out} dt \times F}{\int_0^t C_{CH_4,in} dt \times F - \int_0^t C_{CH_4,out} dt \times F} \quad (2)$$

Average CO selectivity:

$$S_{CO} (\%) = \frac{\int_0^t C_{CO,out} dt \times F}{\int_0^t C_{CH_4,in} dt \times F - \int_0^t C_{CH_4,out} dt \times F} \quad (3)$$

Average CO₂ selectivity:

$$S_{CO_2} (\%) = \frac{\int_0^t C_{CO_2,out} dt \times F}{\int_0^t C_{CH_4,in} dt \times F - \int_0^t C_{CH_4,out} dt \times F} \quad (4)$$

Average coke selectivity:

$$S_{Coke} (\%) = 1 - S_{CO} (\%) - S_{CO_2} (\%) \quad (5)$$

Average H₂ yield:

$$Y_{H_2} = \frac{\int_0^t C_{H_2,out} dt \times F}{R \times m_{cat}} \quad (6)$$

Average CO₂ conversion:

$$X_{CO_2} (\%) = \frac{\int_0^t C_{CO_2,in} dt \times F - \int_0^t C_{CO_2,out} dt \times F}{\int_0^t C_{CO_2,in} dt \times F} \quad (7)$$

Average CO yield:

$$Y_{CO} = \frac{\int_0^t C_{CO,out} dt \times F}{R \times m_{cat}} \quad (8)$$

Average carbon capacity:

$$Y_{Coke} = \frac{\int_0^t C_{CH_4,in} dt \times F - \int_0^t C_{CO,CO_2,CH_4,out} dt \times F}{R \times m_{cat}} \quad (9)$$

Where C is real time volume concentration of gas, F is the gas flow rate,

R is the volume of gas under standard conditions (22.4 L mol⁻¹).

3. Results and discussion

3.1. Catalytic activity and stability

The results of CH₄-TPR and CO₂-TPO were displayed in Fig. 1a and b, respectively, and the evolution of the gas composition of CH₄-TPR with different catalysts was depicted in Fig. S1. The CH₄-TPR results indicated that the catalysts started to react slightly with CH₄ at approximately 300 °C and the reactivity increased with increasing temperature, with the lower initial methane activation temperature indicating some low temperature activity. As shown in Fig. 1(a), the monometallic 25Ni catalyst showed relatively higher activity than all the bimetallic catalysts and the monometallic 25Co catalyst at temperatures lower than 600 °C. This indicated that the Ni species in the catalysts exhibited higher activity for methane cracking than Co species, and higher content of Co species would reduce the activity for methane cracking at low temperatures. Meanwhile, temperature strongly affected catalytic methane conversion. As can be seen from the results of CO₂-TPO for the investigation of the carbon species reactivity with CO₂ (Fig. 1b), the reaction with CO₂ was initiated by all catalysts at approximately 450 °C and with increasing reaction temperature, the CO concentration peaked (at about 700 °C) and then began to drop, indicating that the optimal reaction temperature for carbon removal would be 700 °C. The highest CO peak for catalyst 25Co was approximately 600 °C, suggesting that Co facilitates the reaction of deposited carbon with CO₂. Besides, the largest peak area of CO concentration for the 17Ni8Co catalyst also indicated the best activity. These results illustrated that the carbon species on the catalyst readily reacted with CO₂ in the presence of Co.

The performance of chemical looping CH₄-CO₂ conversion reaction was tested at a constant temperature of 700 °C for all samples, and a CH₄-N₂-CO₂-N₂ process was referred as a CH₄-CO₂ redox test. Significant differences were observed in the thermostatic activity of the catalysts with varying Ni/Co ratios. The instantaneous CH₄ conversion over these catalysts at different reaction time were shown in Fig. 1c. All prepared samples initially displayed high methane conversions, but a slight decline in methane conversion was obtained with the reaction proceeding. It is noted that both the monometallic 25Ni and 25Co catalysts exhibited a sharp decrease in CH₄ conversion, while the decrease is relatively gradual for the bimetallic catalysts. It is also observed that the relatively content of Co species can reduce the initial activity of catalysts. Among all samples, the 17Ni8Co sample demonstrated the best performance with the slowest decline rate in methane conversion and longest time for methane cracking.

In the CO₂ splitting stage, the instantaneous CO₂ conversions over various catalysts were provided in Fig. 1d. The CO₂ conversions in the CO₂ decomposition stage were in consistence with the CH₄ conversions in the methane splitting stage. The CO₂ reaction occurred rapidly over catalysts in the initial stage and basically complete conversions of CO₂ were achieved. As the reaction continued, the catalyst gradually depleted in the methane conversion stage by depositing carbon, and the CO₂ conversion rate gradually decreased. The monometallic Ni and Co catalysts showed the fastest decrease in CO₂ conversion, while the 17Ni8Co catalyst maintained a high CO₂ conversion for the longest duration, indicating that Co played a role in both CH₄ conversion and CO₂ decomposition.

By comparing the evolution of the gaseous products during the methane reaction among 25Ni, 17Ni8Co and 25Ni samples (Fig. 2d), it was clear that the reaction products were predominantly hydrogen, suggesting that the cleavage of feed methane occurred primarily over the catalyst to produce hydrogen and deposited carbon. The evolution of the temporal gaseous products at different reaction time during CH₄ conversion stage and CO₂ splitting stage over other catalysts were depicted in Fig. S2. Whereas the H₂ concentration over the monometallic 25Ni and 25Co samples decreased sharply as the reaction

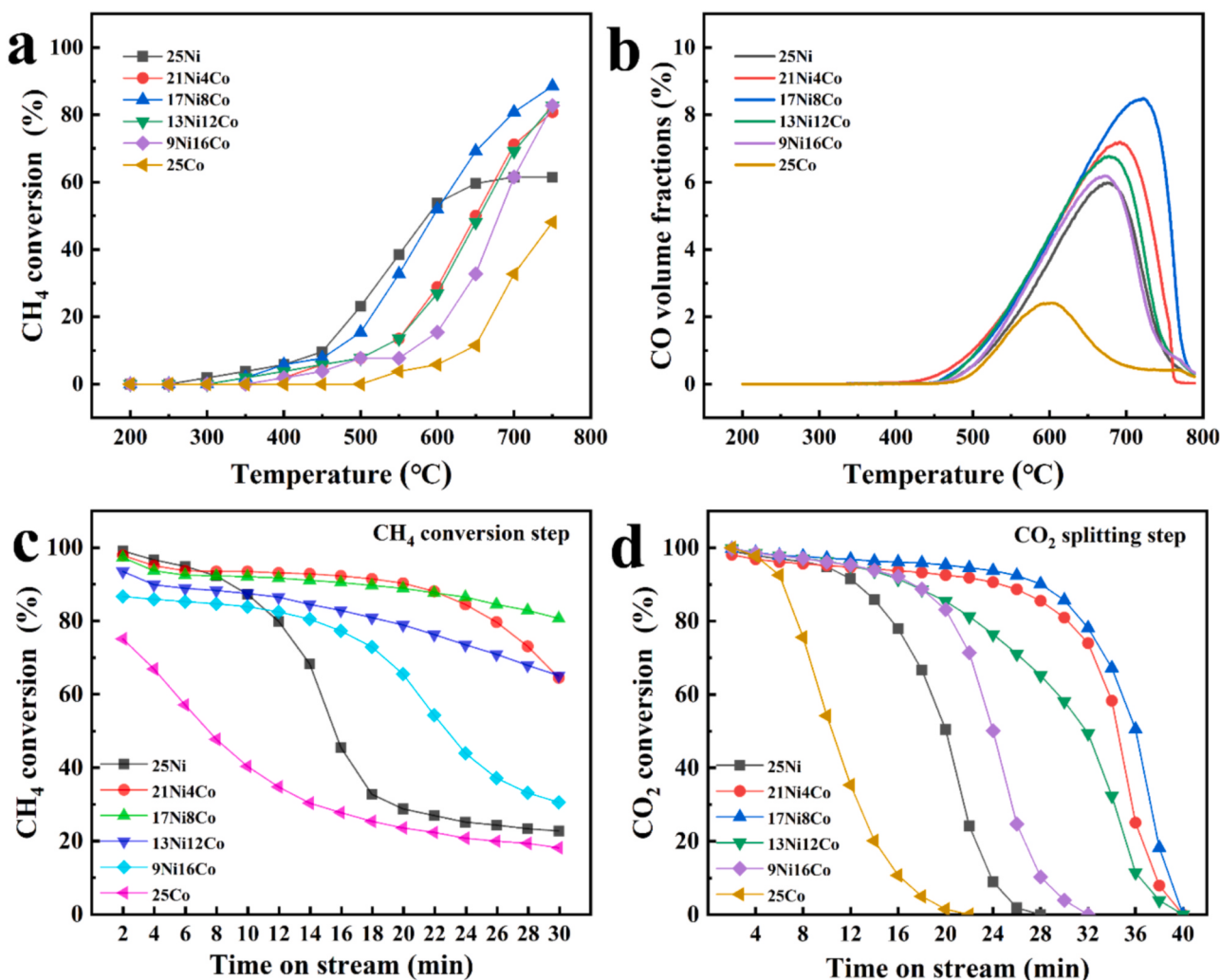


Fig. 1. (a) Temperature-dependent CH₄ transient conversion, and (b) CO₂-TPO profiles of various reduced Co-Ni/Al₂O₃ catalysts. (c) Transient conversion of CH₄ during the cracking reaction at 700 °C, and (d) CO₂ instantaneous conversion during following the CO₂ splitting reaction.

proceeded, accompanied by a rapid increase in CH₄ concentration. The catalyst 17Ni8Co shown a slow decrease in H₂ concentration and a slight increase in CH₄ concentration, potentially due to the synergistic effect of Ni and Co. As the methane cracking reaction progressed, the rise in methane concentration after 15 min clearly led to a sharp decrease in methane conversion (Fig. 1c) due to the gradual accumulation of carbon deposits covering the active site. Consequently, in the following cyclic stability tests, the reduction time was limited to 15 min to ensure satisfactory conversion. Moreover, the H₂ concentration increased sharply to the highest value over 17Ni8Co at the instant of methane feeding and remained stable for a period of time, indicating that the prepared catalyst had a high reaction activity and rate. It was also clear from the quantitative calculations of carbon capacity during the CH₄ conversion step (Fig. 2c) that the carbon capacity of the Co-modified bimetallic catalysts increased significantly, with sample 17Ni8Co displaying the highest carbon capacity (23.59 mol/kg).

For the evaluation of the catalysts, the quantitative analysis of methane conversion step and CO₂ splitting step on different catalysts were shown in Fig. 2a and b. All samples displayed high H₂ selectivity and coke selectivity owing to the fact that methane cracking mainly occurred to produce C and H₂ in the methane conversion stage, with the highest methane conversion (89.5%) and highest H₂ yield (47.9 mol/kg) over sample 17Ni8Co. In the CO₂ splitting stage, the incoming CO₂ reacted with the carbon deposited on the catalyst to form CO, so the highest methane conversion rate of sample 17Ni8Co corresponded to the

highest CO yield. Based on the results of isothermal experiments, the bimetallic catalyst activity was superior to that of the monometallic catalyst, with the bimetallic sample 17Ni8Co exhibiting the best catalytic activity among all the samples, suggesting that the synergy interaction of the two metals was responsible for the enhanced catalytic performance.

To further investigate more about the application potential, 50 redox cycling experiments were performed on the sample 17Ni8Co. In the long-term stability test, no significant changes in CH₄ conversion, H₂ selectivity, coke selectivity and H₂ yield were observed (Fig. 3), confirming the stability of the carbon cycle under mild reaction conditions. In contrast, the catalyst 25 Ni was poorly stabilized and quickly lost activity in successive redox experiments (Fig. S3). The Ni-Co metals played a major catalytic role in converting methane to hydrogen and deposited carbon, while reducing carbon dioxide to CO by eliminating carbon species deposited on the catalyst surface. This could solve the problems caused by the limited release of lattice oxygen from the conventional metal oxides and the unsatisfactory reduction kinetic rate. The XRD results of the fresh and recycled catalysts (Fig. S4) as well as the spent and regenerated catalysts (Fig. 5b) demonstrated the satisfactory circularity in the elimination and regeneration of deposited carbon species and the stability of the crystalline phase. Furthermore, the EDS mapping (Figs. 7b₃ and 8b₄) showed a uniform spatial distribution of Ni-Co elements supported by an Al₂O₃ carrier. The superior activity and stability of the catalyst in successive cycling experiments might be

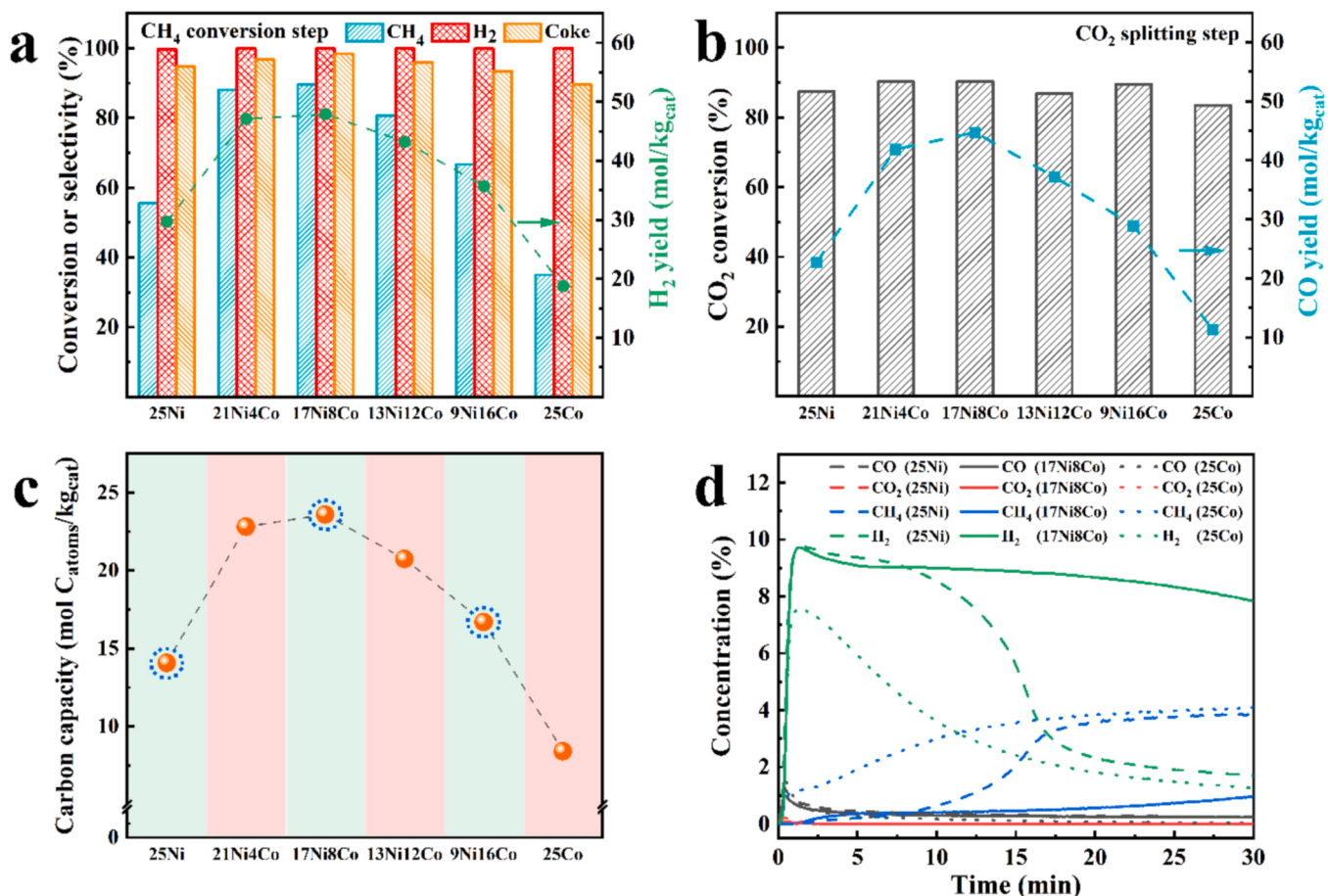


Fig. 2. Isothermal test results of catalyst Co-Ni/Al₂O₃. (a) CH₄ conversion, H₂ and coke selectivity and H₂ yield during the CH₄ conversion step. (b) CO₂ conversion and CO yield during the CO₂ splitting step. (c) Carbon species capacity during the CH₄ conversion step. (d) Evolution of temporal gaseous products upon the reaction of 25Ni and 17Ni8Co with CH₄.

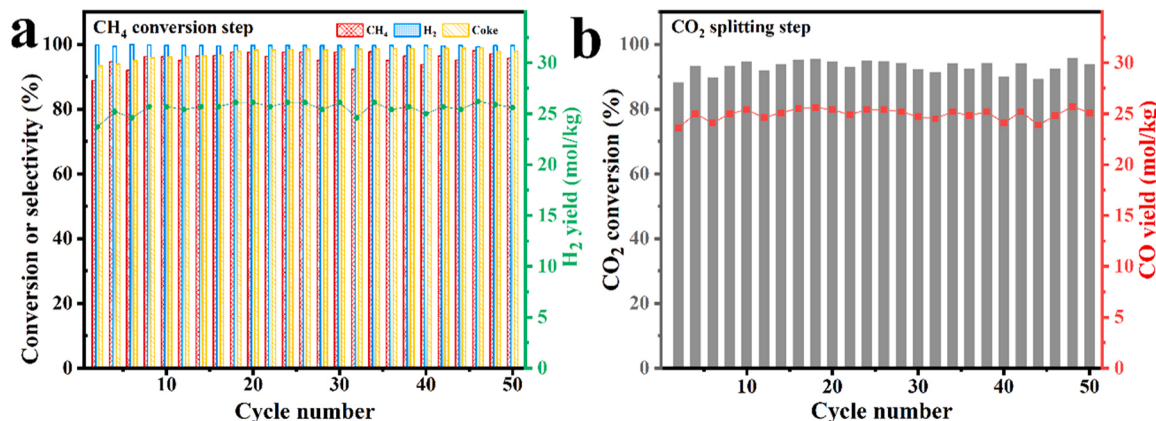


Fig. 3. Cycle stability of the 17Ni8Co catalyst over 50 consecutive redox cycles during CH₄-CO₂ splitting at 700 °C: (a) CH₄ conversion, H₂ and coke selectivity and H₂ yield during the CH₄ conversion step, (b) CO₂ conversion and CO yield during the CO₂ splitting step.

attributed to the interaction between the metals in the catalyst.

3.2. Structure and reducibility of catalysts

The XRD analyses of all prepared fresh samples were shown in Fig. 4a. The diffraction peaks of both the monometallic and bimetallic catalysts were relatively sharp, implying the high crystallinity of the prepared samples. The fresh monometallic sample 25Co and 25 Ni displayed a clear characteristic diffraction peak of Co₃O₄ and NiO,

respectively. The XRD pattern from 25° to 45° for the fresh samples tested showed a decreasing trend in the intensity of the NiO diffraction summits at about 43° and 62° with decreasing loading of Ni in the catalyst. Similarly, the characteristic peak intensity of Co₃O₄ also varied regularly with the change in content.

The XRD pattern of the reduced sample after H₂ flow was given in Fig. 4c. The two minor diffraction peaks at 45.8° and 66.8° were all from Al₂O₃ support, corresponding to the (400) and (440) crystal planes, respectively. The three distinct diffraction peaks at about 44° (111), 51°

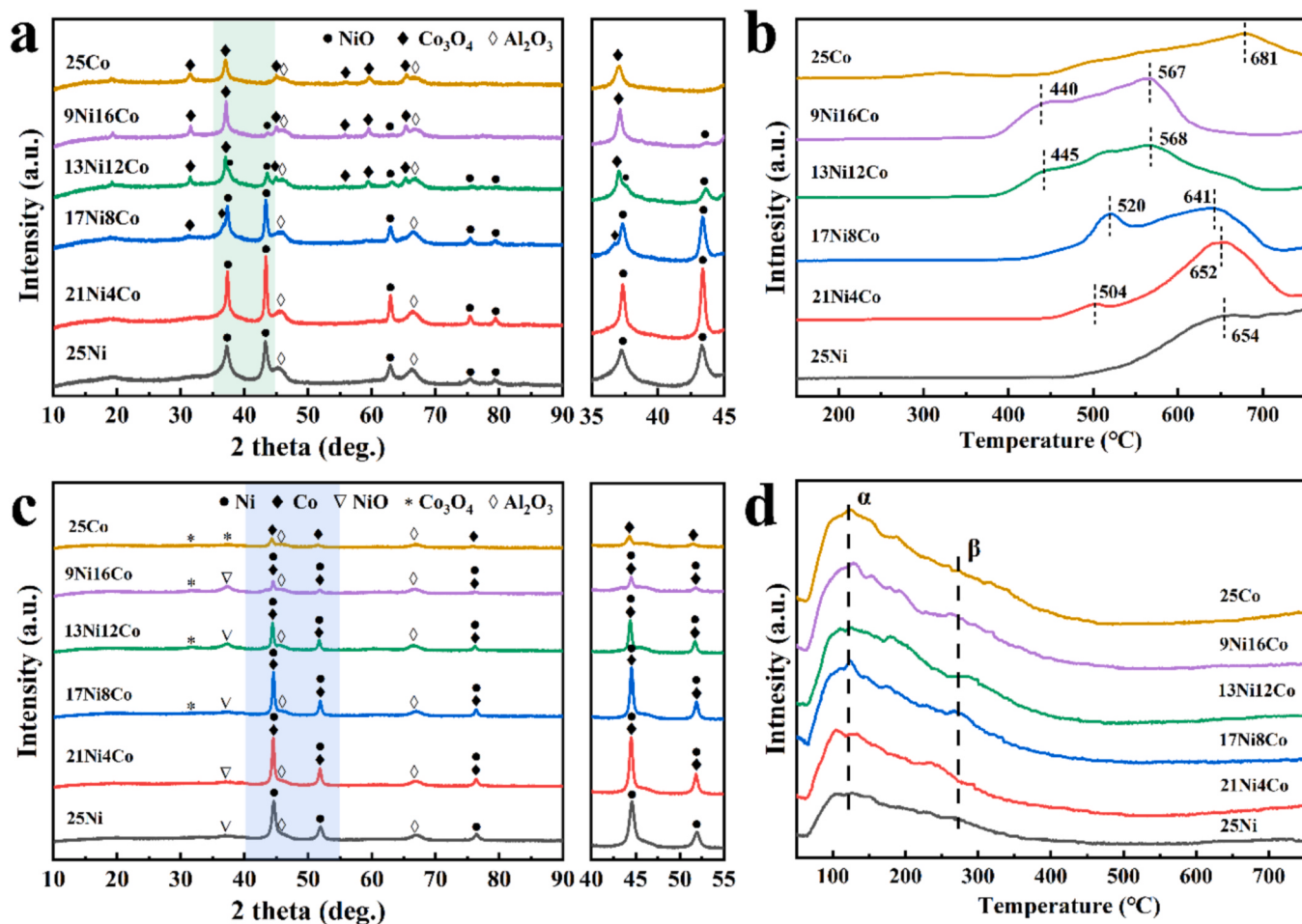


Fig. 4. XRD patterns of the fresh (a) and H₂ reduced (c) catalysts. H₂-TPR profiles (b) and CO₂-TPD profiles (d) of the fresh catalysts.

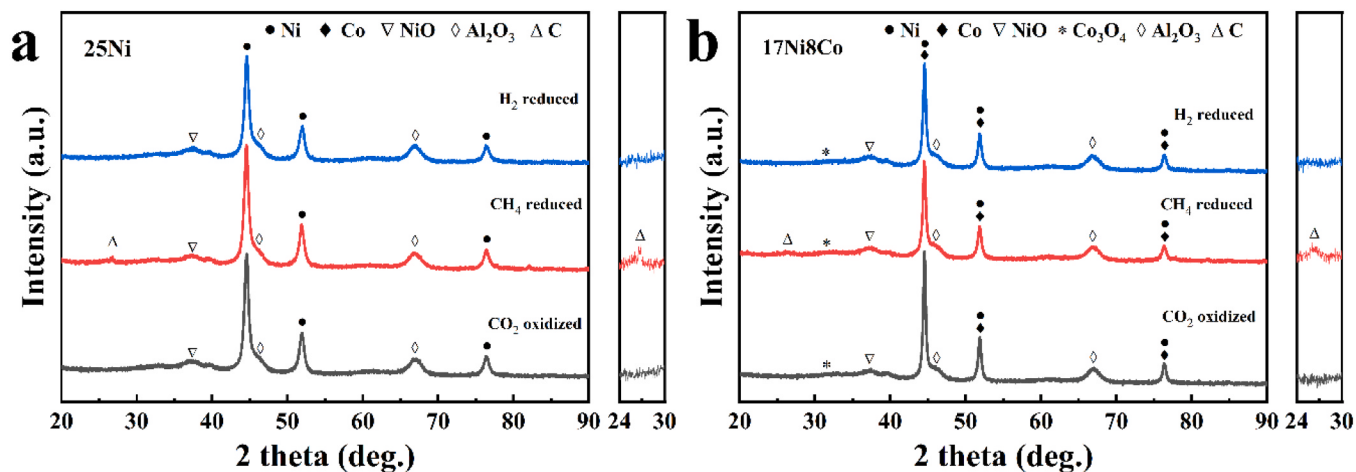


Fig. 5. XRD patterns of H₂-reduced, CH₄-reduced and CO₂-oxidized samples for 25Ni (a) and 17Ni8Co (b).

(200) and 76° (220) could be attributed to metallic Ni, Co or Ni-Co alloys [20,32]. Additionally, the two weak diffraction peaks at about 37° and 31° were due to the formation of NiO with Co₃O₄ in air. The shifting of the positions of diffraction peaks at about 44° (111) and 51° (200) was correlated to the presence of Co in the catalysts [30]. In general, since Co has a slightly larger atomic radius than Ni (3.55 Å vs. 3.52 Å), the substitution of Ni by Co would result in the shift of the diffraction peaks to the lower 2θ positions based on the Vegard's law [22,33]. Fig. S5

showed a plot of lattice parameters versus Ni/Co composition. The strongest diffraction peak of all bimetallic catalysts was located at about 44.4°, between the diffraction peaks of metals Co and Ni, which indicates the formation of Ni-Co alloys [20]. Furthermore, step-scan XRD from 40° to 45° clearly demonstrated the presence of the Ni-Co phase and the position of the Ni-Co peak varied regularly with the Co content.

The H₂-TPR results for all catalysts were shown in Fig. 4b. Collectively, the H₂ reduction peaks for all samples became larger with

increasing temperature. The H₂ consumption peaks at low temperatures for the monometallic samples 25Ni and 25Co were likely attributed to the reduction of free small particles of NiO and Co₃O₄, along with the remaining bulk Ni(Co) oxides being further reduced with increasing temperature, while the H₂ consumption peaks at high temperatures (>700 °C) indicated the existence of strong interactions between the Ni (Co) oxides and support [34–38]. For bimetallic catalysts, the appearance of H₂ consumption in the 400–500 °C range might be attributed to the reduction of Co³⁺, Ni²⁺ and Co²⁺, which might occur simultaneously. Between 500 °C and 700 °C, the remaining massive intractable Ni and Co oxides were further reduced to Ni⁰ and Co⁰ [22,37]. The reduction temperatures for Ni-Co catalysts were relatively lower in contrast to the single Co or Ni catalysts. This indicated that the formation of Ni-Co alloy may weaken the interaction between Co or Ni species with the support, thus enhancing the reducibility of alloy catalysts at lower temperatures. The CO₂-TPD of the catalysts were shown in Fig. 4d.

Clearly, two desorption peaks α and β were observed for all samples at low temperatures, and no other desorption peaks were found at high temperatures. The desorption peak α tended to become larger with enhanced Co content, indicating that Co contributed to the adsorption of CO₂, which could facilitate the elimination of carbon deposition on the catalyst surface. Further, the 25Ni and 17Ni8Co samples were characterized and discussed in detail.

3.3. Metal valence of catalysts

The XRD results for samples 25Ni and 17Ni8Co indicated no significant changes for the samples before and after the reaction (Fig. 5), confirming the crystalline phase stability. It is worth noting that after the reduction reaction with methane, graphitic carbon (002) was formed on the spent catalyst with the diffraction peak at approximately 26° and disappeared after oxidation by CO₂, as shown in the local magnification

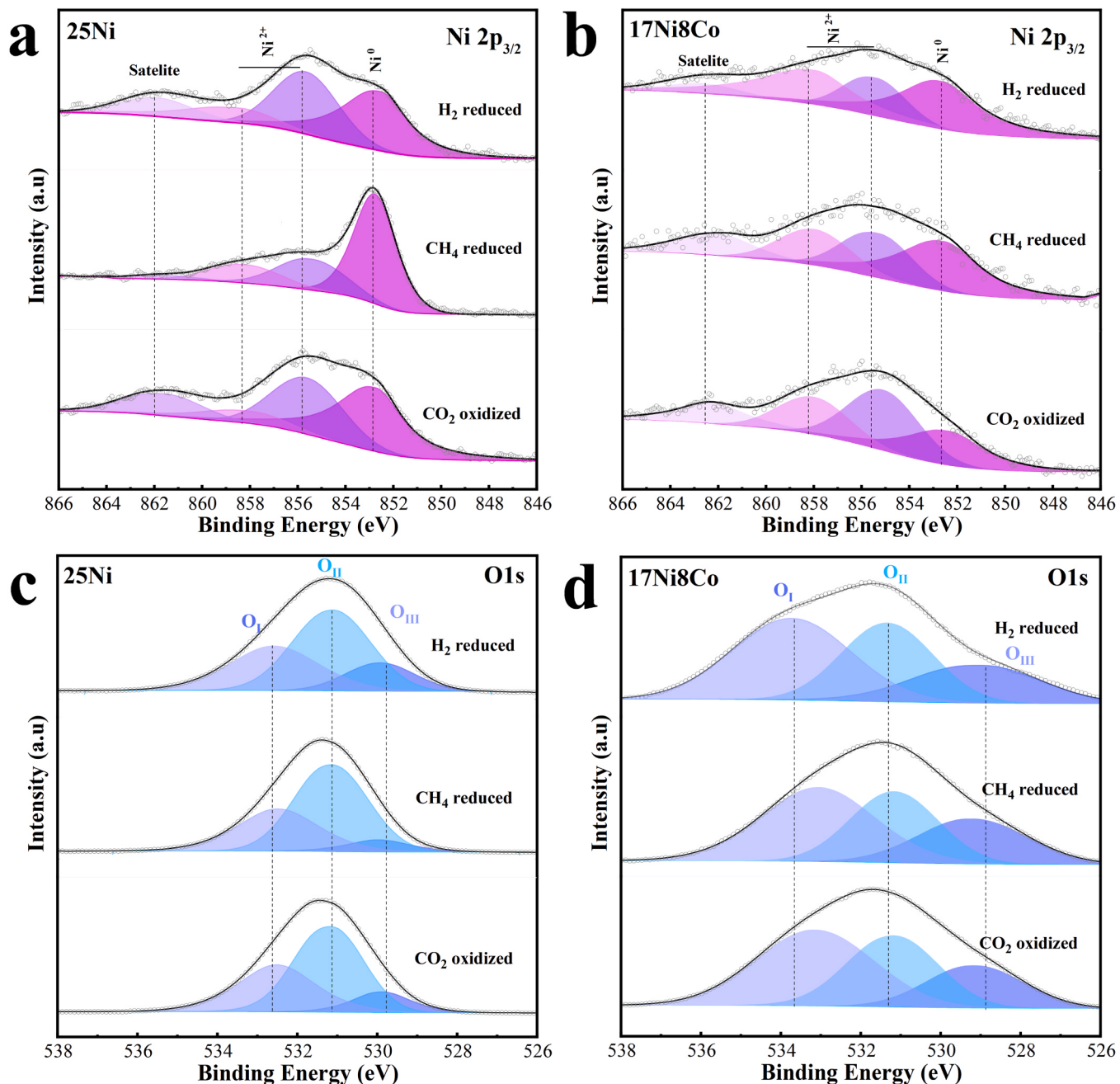


Fig. 6. XPS spectra of O 1s and Ni 2p_{3/2} over 25Ni and 17Ni8Co catalysts in various steps.

pattern of $2\theta=24-26^\circ$. The majority of deposited carbon could possibly be eliminated, and the remaining trace carbon species may make it difficult to detect by XRD.

As the electronic state on the surface of the catalyst had a great influence on the catalytic process, XPS was employed to study the changes in the surface chemical state of catalysts 25Ni and 17Ni8Co at various steps (Fig. 6). Ni^0 was present in the catalysts around 852 eV, except for metallic Ni oxidized by air and Ni^{2+} generated by strong interaction with the support (Al_2O_3).

The relatively high concentration of Ni^0 species in either catalyst 25Ni (CH_4 reduced) or 17Ni8Co (CH_4 reduced) could result from the encapsulation of carbon deposition, which might prevent the oxidation of Ni^0 by air. Therefore, nickel was more oxidized in the bimetallic samples compared to the monometallic oxides, which could be due to the charge transfer from nickel to cobalt [22]. The effect of Ni-Co alloying on the surface oxygen properties of the redox catalysts was also investigated by XPS. The O_{III} (~529 eV) and O_{I} (~533 eV) peaks could be attributed to the lattice oxygen (O_{latt}) and surface adsorbed oxygen (O_{ads}), respectively, while OII (~531.1 eV) was assigned to the oxygen in the carrier Al_2O_3 . O_{latt} was related to the lattice oxygen owing to the oxidation of metallic Ni, Co or Ni-Co alloys by air, whereas O_{ads} might be attributed to hydroxyl groups (OH^-) and/or carbonates (CO_3^{2-}). The bimetallic 17Ni8Co catalyst contained more O_{latt} or O_{ads} than the monometallic 25Ni, which could be ascribed to the oxygenophilic nature of Co.

3.4. Growth and elimination of carbon deposition

The microscopic morphological structure of fresh 25Ni and 17Ni8Co catalysts was characterized by TEM (Fig. 7). The flocculent agglomerate with a dark and light dispersed layout of colors was observed for the samples (Fig. 7a₂ and b₂). The darker areas represented the active component metals Ni and Co, and the lighter filamentous species were fibrous Al_2O_3 .

The Ni and Ni-Co catalysts showed large spherical particles, and the

average particle size of the Ni-Co catalyst was found to be much larger than that of the pure Ni catalyst. The STEM/EDS mapping images of catalyst 17Ni8Co (Fig. 7b₃) displayed the same spatial distribution of Ni and Co, while the XRD results indicated the incorporation of cobalt into the nickel lattice to form Ni-Co alloy particles. The formation of Ni-Co alloy configurations may dramatically influence the electronic properties of Ni/Co metals in favor of the catalytic properties [28].

To further investigate the morphology and organization of the 25Ni and 17Ni8Co catalysts after the methane flow reaction, TEM measurements were performed (Fig. 8). The presence of carbon cladding with ordered carbon streaks was also proved in the high-resolution TEM images of dark metallic grained surfaces (Fig. 8a₄ and b₃), also as evidenced by the line scan images. The surface scan results (Fig. 8b₄) further demonstrated the stable presence of the Ni-Co alloy phase in the catalyst. Based on the TEM images of samples 25Ni and 17Ni8Co after reaction with CH_4 (Fig. 8c₁-c₃, d₁ and d₂), a significant difference in the thickness of the outer carbon cover layer between particles of different diameters was easily observed, and the size of the particles was supposed to affect the thickness of the accumulated carbon cover layer. Smaller particles with thicker inclusions may lead to the deactivation of the active sites of the catalyst resulting in limited carbon capacity, additionally the elimination of carbon build-up by CO_2 may be hampered. In contrast to pure Ni catalyst, the alloyed catalysts with larger particles might enable a relatively thin carbon inlay. In this case, larger Ni particles would be beneficial for prolonging the lifetime of the catalysts. It was also noteworthy that the carbon deposition on the alloyed Ni-Co particles appeared to be bent and wrapped, and its growth was in all directions, with accumulation away from the active site (Fig. 8d₂). The line scan data also revealed the presence of carbon build-up around the Ni-Co particles (Fig. 8b₃), which appeared to prevent the active sites from being rapidly inactivated by the carbon build-up, resulting in a higher carbon capacity of the catalyst (Fig. 2c).

TEM tests were conducted on the regenerated catalyst 25Ni and 17Ni8Co by removing carbon deposits through CO_2 flow. Comparing the methane-reduced samples (Fig. 9), the elimination of the carbon build-

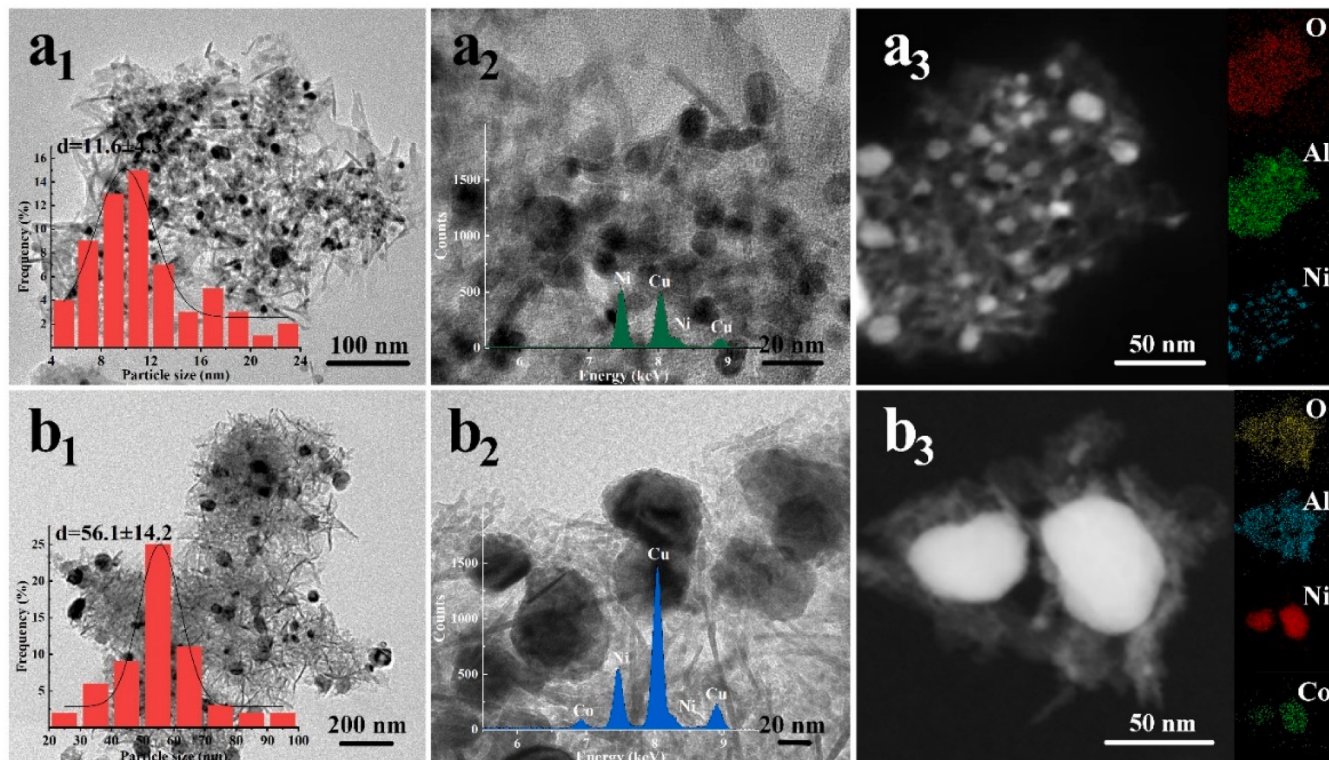


Fig. 7. TEM, High-resolution TEM and STEM/EDS elemental mapping images of fresh catalysts 25Ni (a₁-a₃) and 17Ni8Co (b₁-b₃).

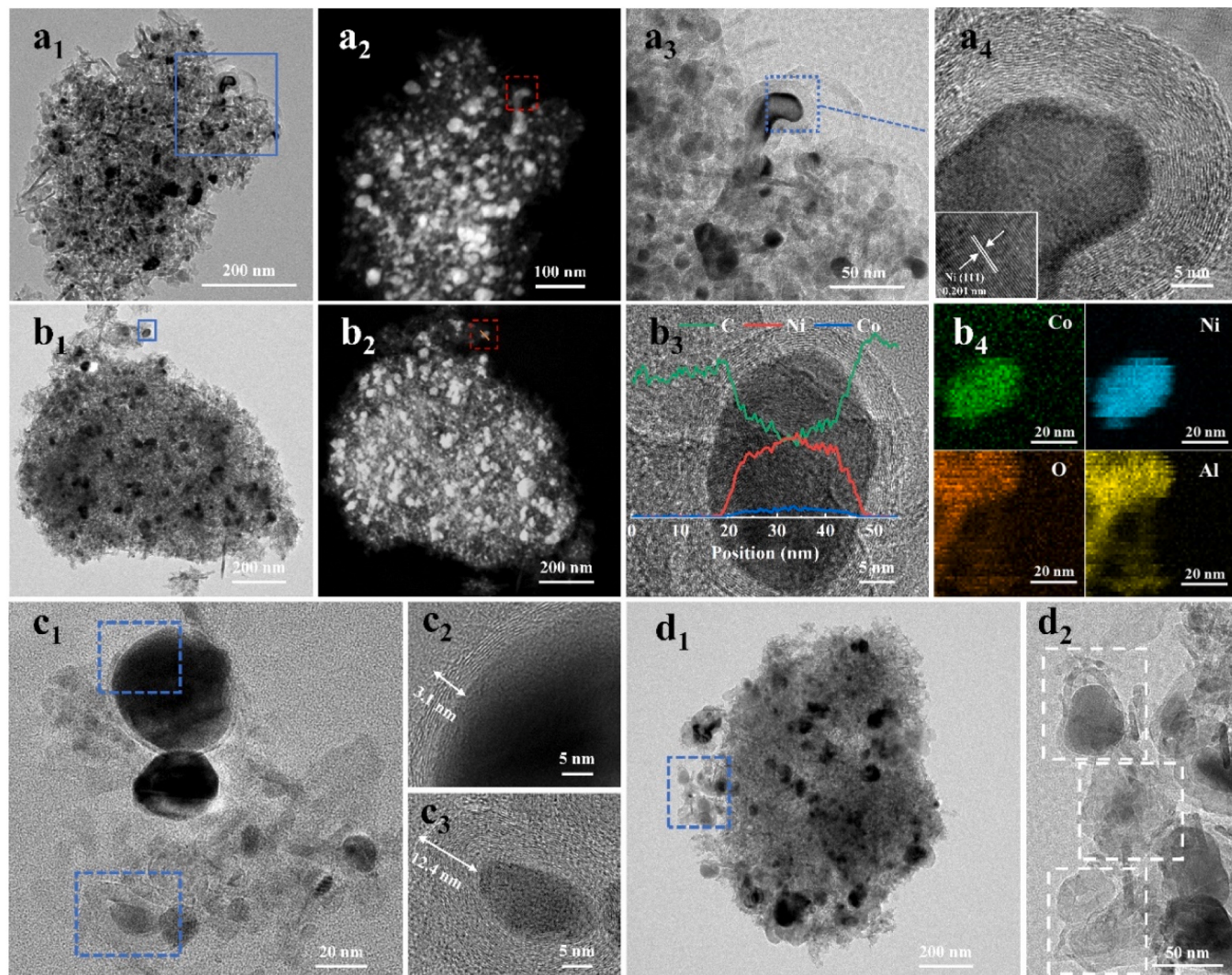


Fig. 8. TEM, High-resolution TEM, STEM/EDS elemental mapping images and line scan of catalysts 25Ni (a₁-a₄, c₁-c₃) and 17Ni8Co (b₁-b₄, d₁, d₂) after the reaction with CH₄.

up encapsulated in the outer layer of the spherical catalyst was clearly observed under high resolution (Fig. 9a₃ and b₃). Furthermore, line scan results of the samples showed that less deposited carbon was left on the Ni-Co alloy surface than on the monometallic Ni surface, suggesting the superior ability of eliminating deposited carbon for the Ni-Co alloy catalyst. Moreover, Raman tests (Fig. S6) displayed that the graphitization of the carbon build-up on the 25Ni catalyst after the reaction was also higher than that on the 17Ni8Co catalyst (comparing I_G/I_D), while the less graphitized carbon build-up made it easier to be removed [17, 39]. The introduction of Co reduced its graphitization, enabling easier removal of carbon deposits. Furthermore, based on the combined CO₂-TPD and CO₂-TPO results, the superior stability of the Ni-Co alloy catalysts was facilitated by the strong ability of Co to adsorb oxygen species owing to its high oxygen affinity. Therefore, the superior stability of the Ni-Co alloy catalysts was achieved in this work.

4. Conclusions

A carbon cycling was employed to replace the oxygen carrier as an intermediate in the chemical looping CH₄-CO₂ redox. The Ni-Co/Al₂O₃ catalysts with metallic components Ni and Co were used to activate CH₄ cracking and CO₂ splitting, and the surface composition of Ni-Co clusters could be modulated by adjusting the ratio of Ni/Co. The results showed that a small amount of Co was sufficient to optimize the regulation,

while too much Co in the catalysts would reduce the methane cracking activity.

The carbon deposits left over from the C-H fracture of CH₄ induced by Ni-Co alloy can be oxidized by the reactive oxygen from Ni-Co catalyzed CO₂ splitting, thus enabling the regeneration of metal surface. The Co alloyed with Ni could produce larger particles and simultaneously influence the growth of the accumulated carbon in a manner that bent it towards the periphery of the active site, avoiding rapid deactivation of the catalyst due to the encapsulation of the active sites with carbon deposits and yielding higher carbon capacities. It can also be concluded that the support may affect the activity and lifetime of methane cracking by tuning the particle size of Ni species and the interaction with Ni. Additionally, the introduction of Co could also enhance the ability of the catalyst to improve CO₂ adsorption and weaken carbon deposits graphitization, whereby promoting the ability of eliminating carbon deposits on the catalyst and stabilizing the catalyst in the long-term reaction.

More importantly, the Ni-Co alloys with appropriate ratio could harmoniously balance the CH₄ cracking rate and CO₂ splitting rate, thereby effectively facilitating carbon deposition and elimination and ensuring the rapid and steady progress of the reactions. Therefore, the Ni-Co/Al₂O₃-assisted carbon cycling process may offer the potential to enhance the splitting and utilization of CH₄ and CO₂.

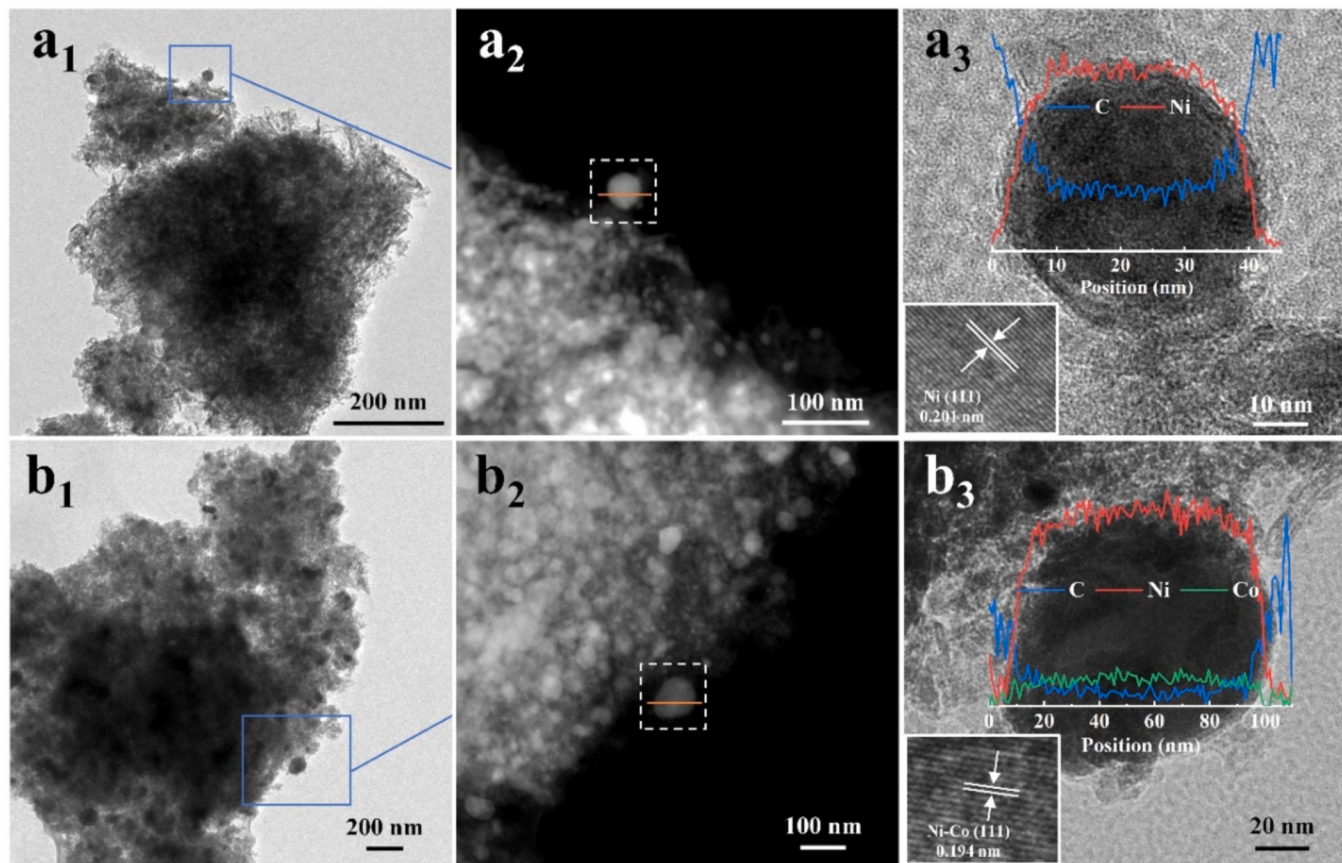


Fig. 9. TEM, High-resolution TEM, STEM/EDS elemental line scan of catalysts 25Ni (a₁-a₃) and 17Ni8Co (b₁-b₃) after the reaction with CO₂.

CRediT authorship contribution statement

Jiangyong Yuan: Conceptualization, Methodology, Visualization, Writing – original draft. **Chunqiang Lu:** Data curation, Investigation. **Zhenhua Gu:** Investigation. **Jun Cai:** Resources, Writing – review & editing. **Han Zhao:** Resources, Writing – review & editing. **Danyang Li:** Investigation. **Lei Jiang:** Investigation. **Haiwen Xu:** Validation. **Zhi qiang Li:** Software. **Kongzhai Li:** Funding acquisition, Writing – review & editing, Supervision.

Declaration of Competing Interest

The authors declare that they have no known competing financial interests or personal relationships that could have appeared to influence the work reported in this paper.

Data availability

Data will be made available on request.

Acknowledgments

This work was financially supported by the National Natural Science Foundation of China (Nos. 52174279, U2202251 and 52266008), the Central Guiding Local Science and Technology Development Fund (No. 202207AA110001) and Major R&D Special Project of Yunnan Province “Research and Application of Catalytic Conversion of CO₂ to High Value Chemicals” (No: 202302AG050005).

Appendix A. Supporting information

Supplementary data associated with this article can be found in the online version at doi:10.1016/j.apcatb.2023.123318.

References

- [1] C. Hepburn, E. Adlen, J. Beddington, E.A. Carter, S. Fuss, N. Mac Dowell, J.C. Minx, P. Smith, C.K. Williams, The technological and economic prospects for CO₂ utilization and removal, *Nature* 575 (2019) 87–97.
- [2] L. Alves, V. Pereira, T. Lagarteira, A. Mendes, Catalytic methane decomposition to boost the energy transition: Scientific and technological advancements, *Renew. Sustain. Energy Rev.* 137 (2021).
- [3] M. Peplow, The race to upcycle CO₂ into fuels, concrete and more, *Nature* 603 (2022) 780–783.
- [4] P. Schwach, X. Pan, X. Bao, Direct conversion of methane to value-added chemicals over heterogeneous catalysts: challenges and prospects, *Chem. Rev.* 117 (2017) 8497–8520.
- [5] A. Beheshti Askari, M. Al Samarai, B. Morana, L. Tillmann, N. Pfander, A. Wandzilak, B. Watts, R. Belkhouri, M. Muhrer, S. DeBeer, In situ X-ray microscopy reveals particle dynamics in a NiCo dry methane reforming catalyst under operating conditions, *ACS Catal.* 10 (2020) 6223–6230.
- [6] S. Tian, F. Yan, Z. Zhang, J. Jiang, Calcium-looping reforming of methane realizes in situ CO₂ utilization with improved energy efficiency, *Sci. Adv.* 5 (2019), eaav5077.
- [7] D. Pakhare, J. Spivey, A review of dry (CO₂) reforming of methane over noble metal catalysts, *Chem. Soc. Rev.* 43 (2014) 7813–7837.
- [8] X. Zhang, C. Pei, X. Chang, S. Chen, R. Liu, Z.J. Zhao, R. Mu, J. Gong, FeO₆ octahedral distortion activates lattice oxygen in perovskite ferrite for methane partial oxidation coupled with CO₂ splitting, *J. Am. Chem. Soc.* 142 (2020) 11540–11549.
- [9] J. Yang, E. Bjørgum, H. Chang, K.-K. Zhu, Z.-J. Sui, X.-G. Zhou, A. Holmen, Y.-A. Zhu, D. Chen, On the ensemble requirement of fully selective chemical looping methane partial oxidation over La-Fe-based perovskites, *Appl. Catal. B Environ.* 301 (2022).
- [10] X. Yin, L. Shen, S. Wang, B. Wang, C. Shen, Double adjustment of Co and Sr in LaMnO_{3+δ} perovskite oxygen carriers for chemical looping steam methane reforming, *Appl. Catal. B Environ.* 301 (2022).

- [11] L. Zeng, Z. Cheng, J.A. Fan, L.-S. Fan, J. Gong, Metal oxide redox chemistry for chemical looping processes, *Nat. Rev. Chem.* 2 (2018) 349–364.
- [12] G. Prieto, S. Beijer, M.L. Smith, M. He, Y. Au, Z. Wang, D.A. Bruce, K.P. de Jong, J. Spivey, P.E. de Jongh, Design and synthesis of copper-cobalt catalysts for the selective conversion of synthesis gas to ethanol and higher alcohols, *Angew. Chem. Int. Ed. Engl.* 53 (2014) 6397–6401.
- [13] H.M. Torres Galvis, J.H. Bitter, C.B. Khare, M. Ruitenbeek, A.I. Dugulan, K.P. de Jong, Supported iron nanoparticles as catalysts for sustainable production of lower olefins, *Science* 335 (2012) 835–838.
- [14] V.V. Galvita, H. Poelman, C. Detavernier, G.B. Marin, Catalyst-assisted chemical looping for CO₂ conversion to CO, *Appl. Catal. B Environ.* 164 (2015) 184–191.
- [15] J. Huang, W. Liu, Y. Yang, B. Liu, High-performance Ni–Fe redox catalysts for selective CH₄ to syngas conversion via chemical looping, *ACS Catal.* 8 (2018) 1748–1756.
- [16] S.A. Theofanidis, R. Batchu, V.V. Galvita, H. Poelman, G.B. Marin, Carbon gasification from Fe–Ni catalysts after methane dry reforming, *Appl. Catal. B Environ.* 185 (2016) 42–55.
- [17] Y. Kang, Y. Han, C. Wei, K. Liu, M. Tian, C. Huang, C. Wang, J. Lin, B. Hou, X. Pan, Y. Su, L. Li, R. Zhang, Y. Hao, X. Wang, A novel carbon cycle process assisted by Ni/La₂O₃ catalyst for enhanced thermochemical CO₂ splitting, *J. Energy Chem.* 61 (2021) 297–303.
- [18] A. More, C.J. Hansen, G. Veser, Production of inherently separated syngas streams via chemical looping methane cracking, *Catal. Today* 298 (2017) 21–32.
- [19] Y. Wang, L. Yao, Y. Wang, S. Wang, Q. Zhao, D. Mao, C. Hu, Low-temperature catalytic CO₂ dry reforming of methane on Ni–Si/ZrO₂ catalyst, *ACS Catal.* 8 (2018) 6495–6506.
- [20] B. Zhao, P. Liu, S. Li, H. Shi, X. Jia, Q. Wang, F. Yang, Z. Song, C. Guo, J. Hu, Z. Chen, X. Yan, X. Ma, Bimetallic Ni–Co nanoparticles on SiO₂ as robust catalyst for CO methanation: effect of homogeneity of Ni–Co alloy, *Appl. Catal. B Environ.* 278 (2020).
- [21] L. He, M. Li, W.-C. Li, W. Xu, Y. Wang, Y.-B. Wang, W. Shen, A.-H. Lu, Robust and coke-free Ni catalyst stabilized by 1–2 nm-thick multielement oxide for methane dry reforming, *ACS Catal.* 11 (2021) 12409–12416.
- [22] A.H. Braga, D.C. de Oliveira, A.R. Taschin, J.B.O. Santos, J.M.R. Gallo, J.M. C. Bueno, Steam reforming of ethanol using Ni–Co catalysts supported on MgAl₂O₄: structural study and catalytic properties at different temperatures, *ACS Catal.* 11 (2021) 2047–2061.
- [23] W. Tu, M. Ghoussoub, C.V. Singh, Y.C. Chin, Consequences of surface oxophilicity of Ni, Ni–Co, and Co clusters on methane activation, *J. Am. Chem. Soc.* 139 (2017) 6928–6945.
- [24] H. Yan, S. Yao, W. Liang, S. Zhao, X. Jin, X. Feng, Y. Liu, X. Chen, C. Yang, Ni–Co oxide catalysts with lattice distortions for enhanced oxidation of glycerol to glyceric acid, *J. Catal.* 381 (2020) 248–260.
- [25] J. Wang, Y. Fu, W. Kong, S. Li, C. Yuan, J. Bai, X. Chen, J. Zhang, Y. Sun, Investigation of atom-level reaction kinetics of carbon-resistant bimetallic Ni–Co reforming catalysts: combining microkinetic modeling and density functional theory, *ACS Catal.* 12 (2022) 4382–4393.
- [26] A. Movasati, S.M. Alavi, G. Mazloom, Dry reforming of methane over CeO₂–ZnAl₂O₄ supported Ni and Ni–Co nano-catalysts, *Fuel* 236 (2019) 1254–1262.
- [27] H. Ay, D. Üner, Dry reforming of methane over CeO₂ supported Ni, Co and Ni–Co catalysts, *Appl. Catal. B Environ.* 179 (2015) 128–138.
- [28] Z. Wu, B. Yang, S. Miao, W. Liu, J. Xie, S. Lee, M.J. Pellin, D. Xiao, D. Su, D. Ma, Lattice strained Ni–Co alloy as a high-performance catalyst for catalytic dry reforming of methane, *ACS Catal.* 9 (2019) 2693–2700.
- [29] B. AlSabban, L. Falivene, S.M. Kozlov, A. Aguilar-Tapia, S. Ould-Chikh, J.-L. Hazemann, L. Cavallo, J.-M. Basset, K. Takanabe, In-operando elucidation of bimetallic CoNi nanoparticles during high-temperature CH₄/CO₂ reaction, *Appl. Catal. B Environ.* 213 (2017) 177–189.
- [30] T.-Y. Liang, D. Senthil Raja, K.C. Chin, C.-L. Huang, S.A.P. Sethupathi, L.K. Leong, D.-H. Tsai, S.-Y. Lu, Bimetallic metal–organic framework-derived hybrid nanostructures as high-performance catalysts for methane dry reforming, *ACS Appl. Mater. Interfaces* 12 (2020) 15183–15193.
- [31] Y. Turap, I. Wang, T. Fu, Y. Wu, Y. Wang, W. Wang, Co–Ni alloy supported on CeO₂ as a bimetallic catalyst for dry reforming of methane, *Int. J. Hydrog. Energy* 45 (2020) 6538–6548.
- [32] J. Kang, H. Zhang, X. Duan, H. Sun, X. Tan, S. Liu, S. Wang, Magnetic Ni–Co alloy encapsulated N-doped carbon nanotubes for catalytic membrane degradation of emerging contaminants, *Chem. Eng. J.* 362 (2019) 251–261.
- [33] J.L. Pinilla, S. de Llobet, R. Moliner, I. Suelves, Ni–Co bimetallic catalysts for the simultaneous production of carbon nanofibres and syngas through biogas decomposition, *Appl. Catal. B Environ.* 200 (2017) 255–264.
- [34] A.H. Braga, E.R. Sodré, J.B.O. Santos, C.M. de Paula Marques, J.M.C. Bueno, Steam reforming of acetone over Ni- and Co-based catalysts: effect of the composition of reactants and catalysts on reaction pathways, *Appl. Catal. B Environ.* 195 (2016) 16–28.
- [35] J. Guo, H. Lou, H. Zhao, D. Chai, X. Zheng, Dry reforming of methane over nickel catalysts supported on magnesium aluminate spinels, *Appl. Catal. A Gen.* 273 (2004) 75–82.
- [36] C.N. Ávila-Neto, J.W.C. Liberatori, A.M. da Silva, D. Zanchet, C.E. Hori, F. B. Noronha, J.M.C. Bueno, Understanding the stability of Co-supported catalysts during ethanol reforming as addressed by in situ temperature and spatial resolved XAFS analysis, *J. Catal.* 287 (2012) 124–137.
- [37] S. Andonova, C.N. de Ávila, K. Arishtirova, J.M.C. Bueno, S. Damyanova, Structure and redox properties of Co promoted Ni/Al₂O₃ catalysts for oxidative steam reforming of ethanol, *Appl. Catal. B Environ.* 105 (2011) 346–360.
- [38] Y. Ji, Z. Zhao, A. Duan, G. Jiang, J. Liu, Comparative study on the formation and reduction of bulk and Al₂O₃-supported cobalt oxides by H₂-TPR technique, *J. Phys. Chem. C* 113 (2009) 7186–7199.
- [39] J. Wu, J. Gao, S. Lian, J. Li, K. Sun, S. Zhao, Y.D. Kim, Y. Ren, M. Zhang, Q. Liu, Z. Liu, Z. Peng, Engineering the oxygen vacancies enables Ni single-atom catalyst for stable and efficient C–H activation, *Appl. Catal. B Environ.* 314 (2022).